Research in Astronomy and Astrophysics, 24:045002 (6pp), 2024 April https://doi.org/10.1088/1674-4527/ad2c3f

Cosmological Constraints on Neutrino Masses in Light of JWST Red and Massive Candidate Galaxies

Jian-Qi Liu[1], Zhi-Qi Huang[1,2], and Yan Su[1]
[1] School of Physics and Astronomy, Sun Yat-sen University, Zhuhai 519082, China; huangzhq25@mail.sysu.edu.cn
[2] CSST Science Center for the Guangdong-Hong Kong-Macau Greater Bay Area, Zhuhai 519082, China
Received 2023 November 16; revised 2024 February 19; accepted 2024 February 21; published 2024 March 18

Abstract

The overabundance of the red and massive candidate galaxies observed by the James Webb Space Telescope (JWST) implies efficient structure formation or large star formation efficiency at high redshift $z \sim 10$. In the scenario of a low or moderate star formation efficiency, because massive neutrinos tend to suppress the growth of structure of the universe, the JWST observation tightens the upper bound of the neutrino masses. Assuming Λ cold dark matter cosmology and a star formation efficiency $\in[0.05, 0.3]$ (flat prior), we perform joint analyses of Planck +JWST and Planck+BAO+JWST, and obtain improved constraints $\sum m_\nu < 0.196\,\mathrm{eV}$ and $\sum m_\nu < 0.111\,\mathrm{eV}$ at 95% confidence level, respectively. Based on the above assumptions, the inverted mass ordering, which implies $\sum m_\nu \geqslant 0.1\mathrm{eV}$, is excluded by Planck+BAO+JWST at 92.7% confidence level.

Key words: (cosmology:) cosmological parameters – galaxies: abundances – galaxies: formation – neutrinos

1. Introduction

The standard hot big bang cosmology predicts a cosmic neutrino background (CνB), which decoupled from the thermal bath in the early universe at a temperature ∼MeV. The subsequently redshifted momenta of CνB follow an ultra-relativistic Fermi–Dirac distribution with negligible chemical potential and an effective temperature $1.95(1+z)$K, where z denotes the cosmological redshift. Although direct detection of CνB is yet unrealistic, the existence of CνB has been indirectly confirmed by the observations of primordial abundances of light elements and the cosmic microwave background (CMB).

The difference between the squares of the three mass eigenstates has been measured in neutrino flavor oscillation experiments (Fukuda et al. 1998; Abe et al. 2014). These experiments constrain the sum of masses of three neutrino species, $\sum m_\nu$, to be $\geqslant 0.06$ eV for the normal mass ordering $m_1 \sim m_2 \ll m_3$, and $\geqslant 0.10$ eV for the inverted mass ordering $m_3 \ll m_1 \approx m_2$. Distinguishing between the two mass-ordering scenarios, and hence accurate measurements of the sum of neutrino masses, are important for understanding the origin of neutrino masses.

At $z \approx 1100$ where primary CMB anisotropies are generated, the background temperature is $T \approx 3000\,\mathrm{K} \approx 0.3\,\mathrm{eV}$. If $\sum m_\nu \gtrsim 0.3$ eV, neutrino masses will have an impact on the primary CMB via the early integrated Sachs Wolfe effect. In the late universe, massive neutrinos act as a hot dark matter component, which tends to suppress the growth of large scale structure at small scales ($\lesssim$100 Mpc) and alter the CMB lensing effect. The third generation CMB experiment Planck mission constrained the total neutrino masses to be $\sum m_\nu < 0.241$ eV (TTTEEE + lowE + lensing) at 95% confidence level (CL) in the standard Λ cold dark matter (ΛCDM) model (Aghanim et al. 2020). Further including baryon acoustic oscillation (BAO) data, which breaks the degeneracy between neutrino masses and the background expansion history of the universe, pushes the upper limit of neutrino masses to $\sum m_\nu < 0.121$ eV (95% CL). This upper bound already puts inverted mass ordering under pressure (excluded at 90.2% CL).

The standard cosmological structure and galaxy formation are recently challenged by red and massive candidate galaxies from James Webb Space Telescope (JWST). Labbé et al. (2023) found six candidate massive galaxies (stellar mass 10^{10} solar masses) at $7.4 \leqslant z \leqslant 9.1$. This finding suggests that either the star formation efficiency (SFE) significantly exceeds its typical values in low-redshift galaxies, or the halo mass function is about 2σ higher than the prediction of the standard ΛCDM cosmology (Haslbauer et al. 2022; Wang et al. 2023a; Boylan-Kolchin 2023; Lovell et al. 2023; Qin et al. 2023). Although at the current stage a large SFE cannot be theoretically excluded (Zhang et al. 2022; Qin et al. 2023), a large SFE at $z \gtrsim 7$ tends to enhance the UV radiation from galaxies, causing a faster reionization process that is in tension with observation (Goto et al. 2021; Wold et al. 2022; Lin et al. 2024). For this reason, we will take the more widely accepted conservative assumption of SFE $\lesssim 0.1$, and discuss the cosmological implications. Because massive neutrinos tend to suppress the number of massive halos in which massive galaxies are born, a large $\sum m_\nu$ increases the tension between the ΛCDM model and JWST data. Thus, adding JWST data to

the cosmological analysis, as the present work aims to do, helps to tighten the upper bound of neutrino masses.

This paper is organized as follows. Section 2 constructs the likelihood of massive galaxy counting and describes the numerical tool for the likelihood evaluation. In Section 3 we apply the likelihood to the Labbé et al. (2023) data and obtain Planck+JWST and Planck+BAO+JWST joint constraints on $\sum m_\nu$. Section 4 discusses and concludes.

2. Likelihood of Massive Galaxy Counting

The aim of this section is to extend the likelihood of massive galaxy counting in Wang et al. (2023a), which we sketch below, to massive neutrino models.

To assess the impact of massive neutrinos on galaxy formation, we adopt the extended Press-Schechter ellipsoidal collapse model (Press & Schechter 1974; Sheth et al. 2001; Sheth & Tormen 2002) to compute the expected abundance of dark matter halos. It predicts the halo mass function, which is the comoving halo number density per mass interval, to take the form

$$\frac{dN}{dM} = \frac{\bar{\rho}}{M^2}\frac{d\ln\nu}{d\ln M} f(\nu), \tag{1}$$

Here, $\bar{\rho}$ is the average density of the background and $\nu = \delta_c/\sigma(M, z)$, where $\delta_c = 1.686$ corresponds to the critical linear overdensity and $\sigma(M, z)$ is the mass fluctuation at scale $R = (3M/4\pi\bar{\rho})^{\frac{1}{3}}$. The simulation-calibrated $f(\nu)$ factor is given by

$$f(\nu) = 2A\left(\frac{1}{\nu'^{2q}} + 1\right)\frac{\nu'^2}{2\pi} e^{\frac{-\nu'^2}{2}}, \tag{2}$$

where $\nu' = \sqrt{a}\,\nu$, $a = 0.707$, $A = 0.322$ and $q = 0.3$ (Sheth & Tormen 1999). For massive halos we assume that the fraction of baryonic mass in a massive dark matter halo is $f_b \equiv \Omega_b/\Omega_m$, where Ω_b and Ω_m are the parameters of baryon and matter abundance. The stellar mass M_* is then connected to the halo mass $M_{\rm halo}$ via $M_* = \epsilon f_b M_{\rm halo}$, where ϵ is the SFE. This relation allows to convert a stellar-mass threshold $M_{*,\rm cut}$ to a halo-mass threshold $M_{\rm halo,cut} = \frac{M_{*,\rm cut}}{\epsilon f_b}$. Assuming that each massive halo has a massive central galaxy, we can write the expected number of massive galaxies above the stellar-mass threshold and in a selected comoving volume as

$$\langle N_{\rm th}\rangle = 4\pi f_{\rm sky}\int_{M_{\rm halo,cut}}^{\infty} dM \int_{z_{\rm min}}^{z_{\rm max}} \frac{dn}{dM}\frac{dV}{dz d\Omega}\, dz, \tag{3}$$

where the selected comoving volume is defined by the redshift interval $[z_{\rm min}, z_{\rm max}]$ and the sky fraction $f_{\rm sky}$. Following Wang et al. (2023a) we take $z_{\rm min} = 7$ and $z_{\rm max} = 10$. The survey area is 38 arcmin^2, which gives $f_{\rm sky} = 2.56\times10^{-7}$. The comoving volume per redshift interval per solid angle, $\frac{dV}{dz d\Omega}$, is specified by the cosmology. For the spatially flat ΛCDM model, to a very good approximation, we have

$$\frac{dV}{dz d\Omega} = \frac{c^3}{H_0^3\sqrt{\Omega_m(1+z)^3+1-\Omega_m}} \times\left[\int_0^z \frac{dz'}{\sqrt{\Omega_m(1+z')^3+1-\Omega_m}}\right]^2, \tag{4}$$

where c, Ω_m and H_0 are the speed of light, the total matter (CDM + baryon + neutrinos) abundance parameter and the Hubble constant, respectively.

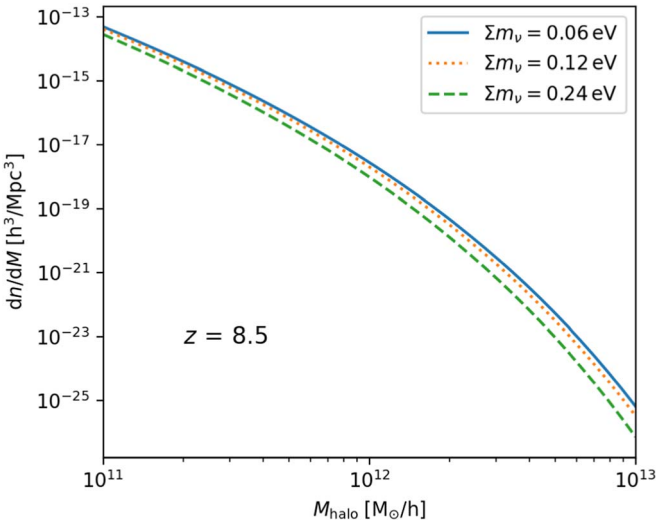

Figure 1. From top to bottom are the halo mass functions at $z = 8.5$ for $\sum m_\nu = 0.06$ eV, 0.12 eV, and 0.24 eV, respectively. The other cosmological parameters (Ω_m, Ω_b, H_0, A_s, n_s) are fixed at Planck best-fit values.

At $z \lesssim 10$, massive neutrinos become non-relativistic and contribute a small ($\sim 10^{-3}$) fraction to the total energy budget of the universe. However, the correction to Equation (4) due to neutrino masses, namely the volume effect, is still negligible for our analysis. The major impact of neutrino masses is on the matter power spectrum, integration of which gives $\sigma(M, z)$ in Equation (1). Figure 1 shows the dependence of halo mass function, evaluated at $z = 8.5$ (the center of the redshift bin used in the likelihood), on the sum of neutrino masses.

The stellar mass and the redshift uncertainties propagate to the uncertainty in $N_{\rm obs}$, the number of observed galaxies above the stellar mass threshold and within the selected volume. Meanwhile, due to cosmic variance and Poisson shot noise, the theoretical prediction of $N_{\rm obs}$ (denoted as $N_{\rm th}$) is also probabilistic. The likelihood of the theory is then characterized by the probability of finding $N_{\rm obs} \leqslant N_{\rm th}$, which is given by

$$P(N_{\rm obs} \leqslant N_{\rm th}) = \sum_{N_{\rm obs}=0}^{\infty} P(N_{\rm obs}) \sum_{N_{\rm th}=N_{\rm obs}}^{\infty} P(N_{\rm th}). \tag{5}$$

The distribution function $P(N_{\rm th})$ is based on the cosmological model and the star formation efficiency. For the purpose of

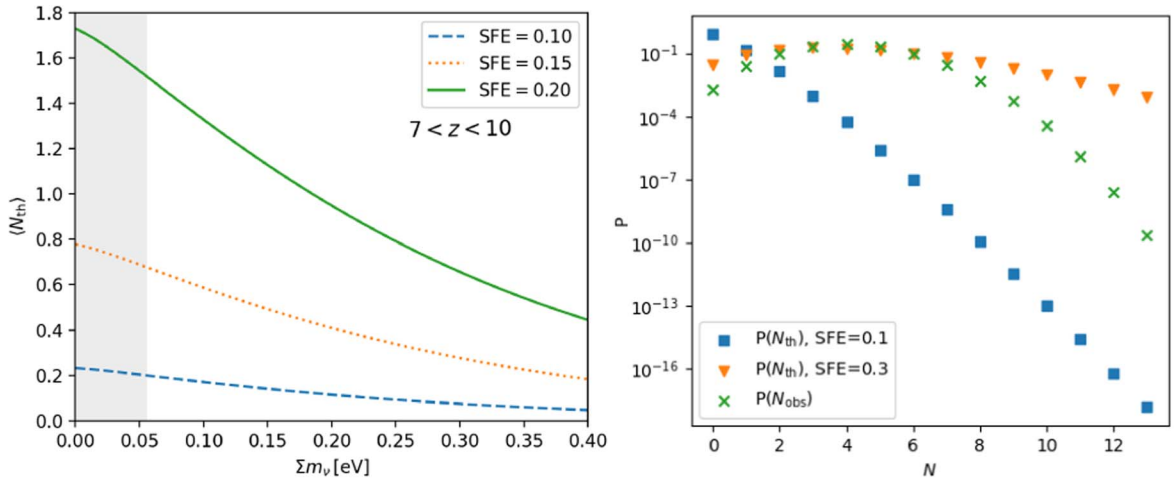

Figure 2. Left panel: dependence of $\langle N_{\rm th}\rangle$ on $\sum m_\nu$ and SFE; other cosmological parameters (Ω_m, Ω_b, h, A_s, n_s) are fixed at the Planck best-fit values. Right panel: $P(N_{\rm obs})$ from the 13 red and massive candidate galaxies in Labbé et al. (2023) and $P(N_{\rm th})$ from the Planck best-fit ΛCDM cosmology.

using rare-object statistics, we are only interested in the $\langle N_{\rm th}\rangle \lesssim O(1)$ case, where $N_{\rm th}$ approximately follows a Poisson distribution. The expectation-value parameter of the Poisson distribution, denoted as λ, has an uncertainty due to cosmic variance (Trenti & Stiavelli 2008). Marginalizing over the cosmic variance of λ that is denoted as σ_λ, we obtain the distribution function of $N_{\rm th}$,

$$P(N_{\rm th}) = \int_{-\infty}^{\infty} \frac{1}{\sqrt{2\pi}\,\sigma_\lambda} e^{-\frac{(\lambda-\langle N_{\rm th}\rangle)^2}{2\sigma_\lambda^2}} e^{-\lambda} \frac{\lambda^{N_{\rm th}}}{N_{\rm th}!} d\lambda. \quad (6)$$

The distribution function $P(N_{\rm obs})$ is obtained by randomly sampling stellar masses and redshifts of the candidate galaxies with the summary statistics given in Labbé et al. (2023), and counting the number of galaxies in the selected volume. The precise values of $P(N_{\rm obs})$ rely on the functional form of the systematic errors of the stellar masses and redshifts of the galaxy candidates. We adopt the triangular distribution function, which is shown to be a more conservative estimation than smooth distributions, e.g., the skew-normal distribution. See Wang et al. (2023a) for more detailed description of the algorithm and its theoretical explanation.

We integrate the cosmological linear perturbation Boltzmann solver CAMB (Lewis et al. 2000; Howlett et al. 2012) into the $P(N_{\rm obs} \leqslant N_{\rm th})$ calculator in Wang et al. (2023a). As shown in the left panel of Figure 2, the expected number of massive galaxies $\langle N_{\rm th}\rangle$ decreases with the sum of neutrino masses, while the other cosmological parameters ($\Omega_m = 0.3158$, $\Omega_b = 0.04939$, $h = 0.6732$, $A_s = 2.101 \times 10^{-9}$, $n_s = 0.9661$) are fixed at the Planck best-fit values (Aghanim et al. 2020). Here the reduced Hubble constant h is defined by $H_0 = 100\,h\,{\rm km\,s^{-1}\,Mpc^{-1}}$; Ω_m and Ω_b are the total matter (CDM + baryon + neutrinos) and baryon abundances; A_s and n_s are the amplitude and spectral index of the power spectrum of the primordial comoving curvature perturbations. In the right panel of Figure 2 we show the derived data, namely $P(N_{\rm obs})$ for the 13 candidate galaxies from Labbé et al. (2023), and the theoretical $P(N_{\rm th})$ for two representative values SFE = 0.1 and SFE = 0.3, respectively. For the case of SFE = 0.1, there is a tension between the theory and the data, as the theory prefers a smaller number of massive galaxies ($N < 2$) than what the data indicates ($N \gtrsim 2$). For SFE = 0.3, the theory is well consistent with the data as $P(N_{\rm th})$ is comparable or greater than $P(N_{\rm obs})$ for all N's.

3. Results

For the given set of observed galaxy candidates and selected volume ($7 \leqslant z \leqslant 10$ and survey area 38 arcmin^2), the cosmology-dependent $P(N_{\rm obs} \leqslant N_{\rm th})$ in Equation (5) gives a likelihood of cosmological parameters and SFE. For more detailed information of the data set, such as the redshifts and stellar masses of the candidate galaxies, we refer the readers to Wang et al. (2023a).

Due to the degeneracy between cosmological parameters, JWST data alone cannot give a meaningful constraint on $\sum m_\nu$. We therefore analyze Planck+JWST and Planck+BAO +JWST jointly by performing importance sampling with the Planck and Planck+BAO Monte Carlo Markov chains from the Planck Legacy Archive (https://pla.esac.esa.int/pla/). The base parameters, on which flat priors are assumed, are the baryon density $\Omega_b h^2$, the CDM density $\Omega_c h^2$, the reionization optical depth τ, the angular extension of sound horizon on the last scattering surface θ, the sum of neutrino masses $\sum m_\nu$, the primordial power spectrum parameters $\ln A_s$ and n_s, and the SFE. Before doing cosmological analysis, we have to assume a prior on SFE. Unless otherwise stated, we focus our study on a

Table 1
Marginalized 1σ Constraints on Cosmological Parameters; for $\sum m_\nu$ the 95% CL Upper Bounds are Shown

	Planck	Planck+JWST	Planck+BAO	Planck+BAO+JWST
$\sum m_\nu$ [eV]	<0.241	<0.196	<0.121	<0.111
σ_8	0.807 ± 0.016	0.811 ± 0.014	0.813 ± 0.010	0.815 ± 0.009
H_0 [km s^{-1} Mpc^{-1}]	67.1 ± 1.05	67.3 ± 0.92	67.8 ± 0.51	67.9 ± 0.50
$100\Omega_b h^2$	2.237 ± 0.015	2.238 ± 0.015	2.242 ± 0.014	2.242 ± 0.014
$\Omega_c h^2$	0.1201 ± 0.0013	0.1200 ± 0.0012	0.1193 ± 0.0009	0.1194 ± 0.0009
100θ	$1.040\,82 \pm 0.00032$	$1.040\,90 \pm 0.00031$	$1.041\,00 \pm 0.00031$	$1.040\,94 \pm 0.00031$
τ	0.0547 ± 0.0076	0.0553 ± 0.0076	0.0553 ± 0.0073	0.0559 ± 0.0073
$\ln(10^{10}A_s)$	3.046 ± 0.015	3.048 ± 0.015	3.045 ± 0.015	3.046 ± 0.015
n_s	0.9648 ± 0.0042	0.9652 ± 0.0042	0.9666 ± 0.0037	0.9667 ± 0.0037

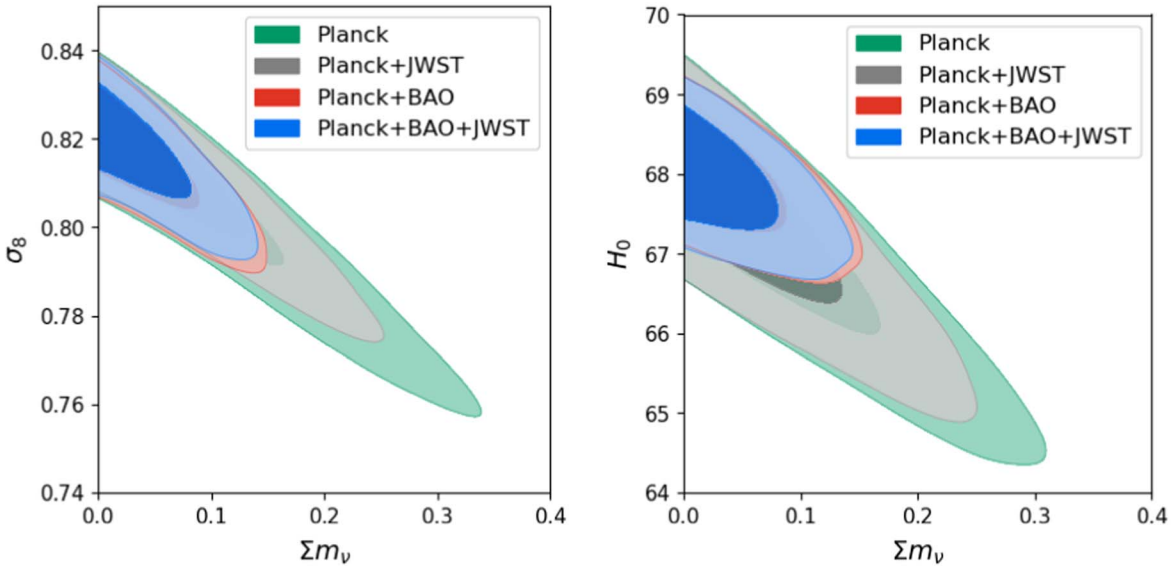

Figure 3. Marginalized 68% CL and 95% CL constraints on ($\sum m_\nu$, σ_8) (left panel) and ($\sum m_\nu$, H_0) (right panel). The units are eV for $\sum m_\nu$ and km s^{-1} Mpc^{-1} for H_0. The prior on star formation efficiency is SFE $\in$ [0.05, 0.3].

low or moderate SFE, namely a flat prior SFE $\in$ [0.05, 0.3], though other options will also be briefly discussed.

The constraints on some key parameters (base or derived), before and after incorporating JWST likelihood, are shown in Table 1 for a comparison. The 95% CL upper bound of $\sum m_\nu$ is improved by 19% (without BAO) and 8% (with BAO), respectively. Although the improvement is insignificant, the inclusion of JWST data pushes the upper bound to $\sum m_\nu < 0.111$ eV, very close to the $\sum m_\nu > 0.1$ eV limit implied by the inverted mass ordering. Integrating over the posterior distribution of $\sum m_\nu$, we find that the inverted mass ordering is excluded by Planck+BAO+JWST at 92.7% CL.

The addition of JWST data also has an impact on σ_8, the root mean square of density fluctuation in a top-hat spherical window with radius $8h^{-1}$ Mpc. This is because the suppression effect due to neutrino masses is degenerate with the amplitude of matter density fluctuations. This degeneracy can be clearly seen in the left panel of Figure 3, which shows the marginalized 1σ and 2σ contours of $\sum m_\nu$ and σ_8. In the right panel of Figure 3 we show the well known geometric degeneracy between $\sum m_\nu$ and H_0, which allows the inclusion of BAO (or any other geometric probes at low redshift) significantly improve the CMB-alone constraint on neutrino masses. The figures are made with the publicly available GetDist package (Lewis 2019).

The solid and filled contours in Figure 4 show the marginalized 1σ, 2σ and 3σ constraints on SFE and $\sum m_\nu$. Although seemingly the upper bound of $\sum m_\nu$ tightens when SFE is lower, it is not the case. This is because the likelihood is very sensitive to SFE, and thus the contours vary significantly when we change the prior on SFE. For example, when the upper bound of SFE is changed to 0.2, the contours become the

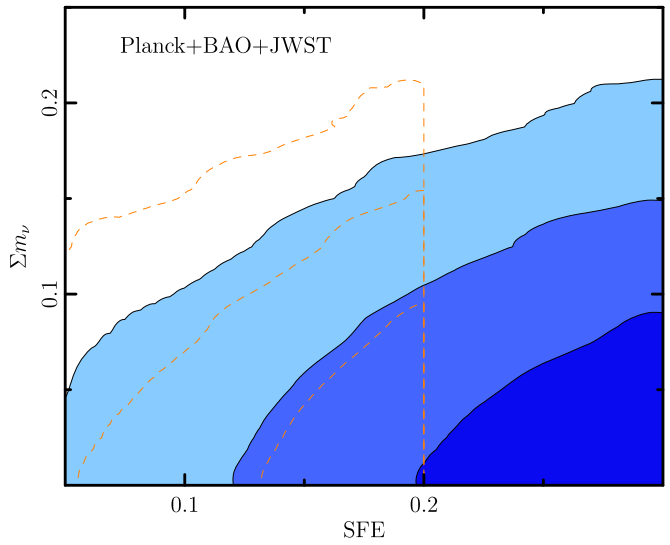

Figure 4. Marginalized 1σ, 2σ and 3σ constraints on SFE and $\sum m_\nu$ with Planck+BAO+JWST. The prior on star formation efficiency is SFE $\in$ [0.05, 0.3]. Orange dashed lines show how the contours vary when the upper bound of SFE is changed to 0.2.

Table 2
Dependence of the 95% CL Upper Bound of $\sum m_\nu$ on the Prior on SFE; Data Sets: Planck+BAO+JWST; the Last Column Shows the Relative Improvement on the $\sum m_\nu$ Bound Against the Planck+BAO (Without JWST) Result, Namely $\sum m_\nu < 0.121$ eV (95% CL)

Prior on SFE	95% CL Upper Bound of $\sum m_\nu$	Improvement Against Planck+BAO
SFE $\in$ [0.05, 0.1]	$\sum m_\nu < 0.118$ eV	2.5%
SFE $\in$ [0.05, 0.2]	$\sum m_\nu < 0.111$ eV	8.3%
SFE $\in$ [0.05, 0.3]	$\sum m_\nu < 0.111$ eV	8.3%
SFE $\in$ [0.05, 0.4]	$\sum m_\nu < 0.114$ eV	5.8%
SFE $\in$ [0.05, 0.5]	$\sum m_\nu < 0.117$ eV	3.3%
SFE $= 0.1$	$\sum m_\nu < 0.114$ eV	5.8%
SFE $= 0.2$	$\sum m_\nu < 0.110$ eV	9.1%
SFE $= 0.3$	$\sum m_\nu < 0.113$ eV	6.6%
SFE $= 0.4$	$\sum m_\nu < 0.118$ eV	2.5%
SFE $= 0.5$	$\sum m_\nu < 0.121$ eV	0%

orange dashed lines in the figure. When we marginalize over SFE, the upper bound of $\sum m_\nu$ does not change much. See also Table 2 for concrete numbers.

By varying the prior on SFE, we also find an interesting phenomenon that, as Table 2 shows, the best improvement of $\sum m_\nu$ bound is achieved around SFE ~ 0.2. Physically this is because a very small SFE makes the likelihood approach a cosmology-independent constant $P \to P(N_{\rm obs} = 0)$, that all candidate galaxies are interpreted as false detections due to systematic errors in redshift and mass, and a very large SFE makes the likelihood approach another cosmology-independent constant $(P \to 1)$, that theoretical prediction significantly exceeds the observed number of galaxies.

4. Conclusions and Discussion

In this work, we incorporate massive neutrinos into the numerical tool in Wang et al. (2023a) to evaluate the likelihood of massive galaxy counting. At the current stage, the JWST candidate galaxies alone cannot constrain cosmology. However, in joint analyses with Planck or Planck+BAO, the addition of JWST massive galaxy counting improves the upper bound of neutrino masses by a few percent and puts the inverted mass ordering under more pressure.

While the Planck+BAO+JWST constraint gives the most stringent upper bound on neutrino masses, the results are yet very model-dependent. In particular, our results rely on SFE prior at $z \sim 7$, namely SFE $\lesssim 0.3$. If a larger SFE $\gtrsim 0.4$, which is unlikely in the usual scenario of galaxy formation and evolution, is assumed, the likelihood becomes insensitive to cosmology and can no longer improve the $\sum m_\nu$ constraint. However, there are alternative scenarios where an enhanced SFE at high redshift does not accelerate the reionization process, and therefore it is consistent with observations. For example, Lin et al. (2024) considered large SFE ($\gtrsim$0.4) at high redshift and warm dark matter in the keV mass range. In this picture, the warm dark matter has no impact on the abundance of very massive halos, and only suppresses the low-mass end of halo mass function. In other words, the keV warm dark matter reduces the number of low-mass galaxies that emit UV photons. This effect cancels the enhancement of UV radiation from each galaxy due to a large SFE, and keeps the cosmic reionization history in line with observations. There are also other options, such as fuzzy dark matter, which can suppress the abundance of small halos and galaxies and lead to the same phenomenon (Gong et al. 2023).

Other cosmological probes, the type Ia supernovae, local distance-ladder measurements of H_0, weak gravitational lensing, redshift-space distortion, etc., may also tighten the current upper bound of neutrino masses. See e.g., Aghanim et al. (2020) and discussion therein. Ideally, one would like to join all the available data and pushes the bound $\sum m_\nu$ to the best limit. However, at the current stage, these cosmological probes, including the JWST high-z massive candidate galaxies, are not all in concordance and may suffer from unknown systematics (Asgari et al. 2021; Riess et al. 2021; Huang et al. 2022; Wang et al. 2023b). It is thus not so favorable to add too many cosmological data into the pool at once, and caution should be taken for the cosmological bounds on neutrino masses. Nevertheless, the growing JWST data bring a hope to cross check the constraints on neutrino masses in very different perspectives (tail statistics, perturbation-based, non-linear physics).

Acknowledgments

This work is supported by the National SKA Program of China No. 2020SKA0110402, the National Natural Science Foundation

of China (NSFC) under grant No. 12073088, and the National Key R&D Program of China (grant No. 2020YFC2201600).

References

Abe, K., Adam, J., Aihara, H., et al. 2014, PhRvL, 112, 061802
Aghanim, N., Akrami, Y., Ashdown, M., et al. 2020, A&A, 641, A6
Asgari, M., Lin, C.-A., Joachimi, B., et al. 2021, A&A, 645, A104
Boylan-Kolchin, M. 2023, NatAs, 7, 731
Fukuda, Y., Hayakawa, T., Ichihara, E., et al. 1998, PhRvL, 81, 1562
Gong, Y., Yue, B., Cao, Y., & Chen, X. 2023, ApJ, 947, 28
Goto, H., Shimasaku, K., Yamanaka, S., et al. 2021, ApJ, 923, 229
Haslbauer, M., Kroupa, P., Zonoozi, A. H., & Haghi, H. 2022, ApJL, 939, L31
Howlett, C., Lewis, A., Hall, A., & Challinor, A. 2012, JCAP, 1204, 027
Huang, L., Huang, Z., Zhou, H., & Li, Z. 2022, SCPMA, 65, 239512
Labbé, I., van Dokkum, P., Nelson, E., et al. 2023, Nature, 616, 266
Lewis, A. 2019, GetDist: A Python Package for Analyzing Monte Carlo Samples, arXiv:1910.13970
Lewis, A., Challinor, A., & Lasenby, A. 2000, ApJ, 538, 473
Lin, H., Gong, Y., Yue, B., & Chen, X. 2024, RAA, 24, 015009
Lovell, C. C., Harrison, I., Harikane, Y., Tacchella, S., & Wilkins, S. M. 2023, MNRAS, 518, 2511
Press, W. H., & Schechter, P. 1974, ApJ, 187, 425
Qin, Y., Balu, S., & Wyithe, J. S. B. 2023, MNRAS, 526, 1324
Riess, A. G., Casertano, S., Yuan, W., et al. 2021, ApJL, 908, L6
Sheth, R. K., Mo, H., & Tormen, G. 2001, MNRAS, 323, 1
Sheth, R. K., & Tormen, G. 1999, MNRAS, 308, 119
Sheth, R. K., & Tormen, G. 2002, MNRAS, 329, 61
Trenti, M., & Stiavelli, M. 2008, ApJ, 676, 767
Wang, J., Huang, Z., Huang, L., & Liu, J. 2023a, arXiv:2311.02866
Wang, J., Huang, Z., & Huang, L. 2023b, SCPMA, 66, 129511
Wold, I. G. B., Malhotra, S., Rhoads, J., et al. 2022, ApJ, 927, 36
Zhang, Z., Wang, H., Luo, W., et al. 2022, A&A, 663, A85